Electromagnetic origins of negative refraction in coupled plasmonic waveguide metamaterials

Iman Aghanejad, Kenneth J. Chau, and Loïc Markley*
The School of Engineering, The University of British Columbia, British Columbia, Canada
(Received 3 March 2016; revised manuscript received 16 September 2016; published 17 October 2016)

A metamaterial composed of stacked plasmonic waveguides which support backward propagation along the layers has been shown to exhibit a nearly spherical equifrequency contour (EFC) in which the Floquet-Bloch wave vector $\mathbf{k}_{FB}$ and Poynting vector $\mathbf{S}$ point in opposite directions everywhere on this surface. Experiments performed on this structure have also shown that polarized light beams incident from free space refract to the same side of normal over a wide range of incidence angles. Together, these observations have led researchers to describe this structure as a homogeneous medium with three-dimensionally isotropic negative refractive index; however, a close inspection of the fields throughout the structure as provided in this paper would suggest otherwise. Here, we rigorously analyze the relationship between phase and power flow within the structure by introducing a method to calculate the power flow of all Floquet-Bloch harmonics, information which cannot be obtained from either conventional analysis of EFCs or effective medium theory. Access to power flow of all harmonics enables us to demonstrate the origin of backward power (defined with respect to the direction of $\mathbf{k}_{FB}$), and in doing so, verify the validity of the claimed three-dimensionally isotropic left-handed response and the validity of describing the medium by a simple negative effective index of refraction $n = -1$. Knowledge regarding the distribution of power flow across the harmonics can also be used to design highly efficient methods to couple light into and out of these structures. As an example, we show that tailored wave excitation can achieve coupling efficiencies of up to 96%, over 5 times greater than that achieved by normal-incidence plane-wave excitation.

DOI: 10.1103/PhysRevB.94.165133

I. INTRODUCTION

Over four decades ago, Veselago proposed a hypothetical homogeneous and isotropic medium with simultaneously negative values of ϵ and μ that could sustain plane waves in which the electric field, magnetic field, and wave vector form a left-handed triad [1]. Plane waves in such an isotropic left-handed (or double-negative) medium are backward waves that propagate with antiparallel phase and group velocities—a condition described by a negative refractive index. In contrast, waves in an isotropic right-handed medium (described by a positive refractive index) propagate with parallel phase and group velocities. In other words, the equifrequency contour (EFC) of the Veselago medium is a sphere whose frequency gradient (the group velocity) points inwards rather than outwards. Energy conservation and phase continuity at a boundary imply that the group velocity (represented by the Poynting vector) and the phase velocity (represented by the wave vector) of a plane wave crossing the interface between an isotropic left-handed medium and an isotropic right-handed medium would refract to the same side of normal, a phenomenon known as negative refraction. In a general homogeneous medium where the condition of isotropy has been relaxed (phase and power are no longer always collinear), negative refraction of phase and negative refraction of power can occur independently and must be treated as independent phenomena. In this situation, the handedness is still defined according to the relative orientations of the wave vector and Poynting vector.

In an effort to mimic the properties of the Veselago medium at optical frequencies, it has been shown that coupling plasmonic waveguides made of metallic and dielectric layers which support backward propagation along the layers can produce a roughly spherical EFC with a radius approximately equal to the free-space wave number [2]. Similar to the Veselago medium, the time-and-space-averaged Poynting vector $\mathbf{S}$ points inwards (backwards) everywhere on this surface. Experimentally, negative refraction of polarized light beams has been observed along planes of incidence parallel (in plane) and perpendicular (out of plane) to the layers [3]. Note that end-fire illumination of a facet perpendicular to the layers can access both planes of incidence, whereas broadside illumination of a facet parallel to the layers can only access the latter (Fig. 1). Snell's law descriptions of measured refraction angles and the effective constitutive parameters extracted by applying a parameter retrieval technique to the simulated reflection and transmission data have also been consistent with approximations of the layered structure as a left-handed (double-negative) medium describable by a three-dimensionally isotropic negative index of refraction $n = -1$ [3]. The mechanism of in-plane negative refraction has been attributed to the guidance of a backward plasmonic mode with opposing phase and group velocities. It is unclear whether out-of-plane negative refraction—where there is the possibility of significant reflection and transmission across layers—is also derived from left-handed modes or if other mechanisms are present. Photonic crystals (with circular EFCs) and indefinite media implemented as metal-dielectric bilayers (with hyperbolic EFCs), for example, provide well-studied cases of structures that exhibit negative refraction of power without left-handed electromagnetic fields [4–6].

We examine the electromagnetic origins of in-plane and out-of-plane negative refraction in a layered plasmonic metamaterial designed by Xu *et al.* that is composed of a periodic repetition of five alternating thin layers of silver and titanium dioxide [3]. This structure is of contemporary interest because it provides the only known template for achieving negative refraction and flat lensing in the ultraviolet, which

*loic.markley@ubc.ca

 ©2016 American Physical Society

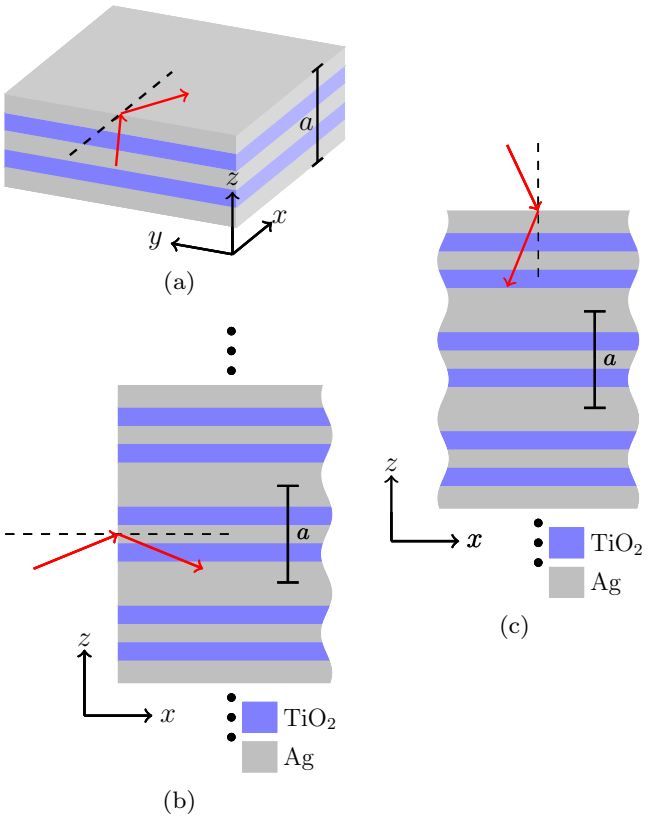

FIG. 1. A diagram illustrating the layered MDMDM structure and the planes of incidence for (a) end-fire in-plane refraction, (b) end-fire out-of-plane refraction, and (c) broadside out-of-plane refraction. The unit-cell periodicity is a.

may be useful for applications such as biological imaging [7,8], photolithography [9,10], plasmonic nanolenses [11], and optical cloaking [12]. The objective of this work is to provide insight into the behavior of electromagnetic modes propagating in the layered structure without making any approximations to the fields. To address this objective from first principles, the electric and magnetic fields inside the medium are calculated from Maxwell's equations, Fourier transformed, and then paired to find the set of Floquet-Bloch harmonics, each with a well-defined wave vector and Poynting vector [13]. A similar expansion has been successfully used to analyze the behavior of the Bloch modes and the origin of negative refraction of power in photonic crystals [14] and left-handedness in magnetodielectric metamaterials [15].

In contrast to homogenization approximations and graphical EFC analyses, which map the properties of a metamaterial onto a single plane-wave mode located in the first Brillouin zone (BZ), our approach maps the properties of a metamaterial onto a spectrum of Floquet-Bloch plane-wave harmonics without loss of information regarding the detailed field variations across each unit cell. In this mapping, we can observe that in general, fields are composed of a mixture of Floquet-Bloch harmonics in which the Poynting vector of each individual harmonic is not aligned to the net power flow and can carry significantly more power than the fundamental harmonic. These facts demonstrate the importance of analyzing higher-order harmonics when studying metamaterials and the need for a method that goes beyond effective medium theory or geometrical EFC analysis. By analyzing the relative directions of phase and power flow of Floquet-Bloch harmonics and finding their individual handedness as a function of propagation direction, we show definitively that in the coupled plasmonic waveguide metamaterial, in-plane backward power arises from left-handed waveguide modes and out-of-plane backward power arises from either left-handed waveguide modes or right-handed scattering effects, depending on the direction of propagation.

Since the fields for out-of-plane propagation contain non-negligible harmonics whose phase velocity components in the direction of propagation are not all identical, the concept of phase refraction and handedness are undefined for the total field (unlike the case of homogeneous media). The average power flow is still clearly defined, however, since it is calculated as the vector sum of all individual harmonic Poynting vectors. Because of this, although there is no clear phase refraction, there is no ambiguity in the all-angle negative refraction of power (or light beams) that was reported in [3]. In this paper, we also rigorously analyze refraction for several different wave incidence scenarios at the end-fire interface to demonstrate the occurrence of both positive and negative refraction of power. We also show that the efficiency of end-fire illumination can be significantly enhanced by choosing alternative excitation channels based on the distribution of power flow across harmonics.

II. FLOQUET-BLOCH MODES IN COUPLED PLASMONIC WAVEGUIDE METAMATERIALS

If we consider a layered metamaterial that is infinite and periodic, the Floquet-Bloch theorem [16,17] states that the field within the metamaterial can be represented as

$$\mathbf{H}(\mathbf{r},t) = \mathbf{u}(\mathbf{r})e^{i(\mathbf{k}_{\mathrm{FB}}\cdot\mathbf{r}-\omega t)}, \tag{1}$$

where $\mathbf{u}(\mathbf{r})$ is a periodic function with the same periodicity as the medium, ω is the frequency, and $\mathbf{k}_{\mathrm{FB}}$ is the complex fundamental Floquet-Bloch wave vector with $\mathbf{k}_{\mathrm{FB}} = \mathbf{k} + i\boldsymbol{\alpha}$. The real part $\mathbf{k}$ is the propagating wave vector and the imaginary part $\boldsymbol{\alpha}$ is the attenuation vector. As attenuation is embedded in the complex Floquet-Bloch wave vector, the function $\mathbf{u}(\mathbf{r})$ represents the nonattenuating periodic component of $\mathbf{H}(\mathbf{r},t)$. Here, we have considered the magnetic field to describe the case of transverse-magnetic (TM) polarization, which is applicable to most plasmonic systems. Substitution of Eq. (1) into the Helmholtz equation yields

$$\nabla\times\left(\frac{1}{\varepsilon}\nabla\times\mathbf{u}\right) + i\mathbf{k}_{\mathrm{FB}}\times\left(\frac{1}{\varepsilon}\nabla\times\mathbf{u}\right) + i\nabla\times\left(\frac{1}{\varepsilon}\mathbf{k}_{\mathrm{FB}}\times\mathbf{u}\right) + \frac{\mathbf{k}_{\mathrm{FB}}\cdot\mathbf{k}_{\mathrm{FB}}}{\epsilon}\mathbf{u} - \frac{\mathbf{k}_{\mathrm{FB}}}{\varepsilon}(\mathbf{k}_{\mathrm{FB}}\cdot\mathbf{u}) - \mu\frac{\omega^2}{c^2}\mathbf{u} = 0, \tag{2}$$

where μ is the relative permeability and ε is the relative permittivity [18]. In order to solve this equation as an eigenvalue problem at a given frequency, constraints must be placed on the Floquet-Bloch wave vector $\mathbf{k}_{\mathrm{FB}}$ so that it can be expressed in terms of a single complex eigenvalue λ. Different constraints are used for different circumstances, with the corresponding eigensolutions unique only to that

constraint. In the case of the infinite layered structure studied in Sec. III, we can define a direction of propagation by choosing $\mathbf{k}_{\mathrm{FB}} = \lambda\hat{\mathbf{k}}$. Equation (2) can be solved for the complex eigenvalue λ and its corresponding eigenmode $\mathbf{u}(\mathbf{r})$ in order to compare the electromagnetic response in different directions of propagation. In the case studied in Sec. IV of refraction across an interface, however, continuity of phase at the interface imposes the constraint on $\mathbf{k}_{\mathrm{FB}}$ and the directions of phase propagation and field decay are no longer necessarily aligned. In this work, both sets of eigenvalue problems are solved using the COMSOL MULTIPHYSICS finite element software package [19].

By convention, we define the equifrequency contour of the metamaterial as the surface traced out by the wave vector $\mathbf{k}$ located in the first Brillouin zone. The EFC and its frequency gradient respectively define the wave vector and group velocity of a plane wave that could be supported by an equivalent homogeneous medium. Taking this analogy further, the process of homogenization assumes that such a homogeneous medium can be used as an effective "black-box" description of the metamaterial.

For TM polarization, a periodic metal-dielectric layered structure can be engineered so that its EFC mimics that of an isotropic left-handed medium [2]. In particular, this has been demonstrated for a unit cell consisting of a MDMDM layer sequence in which the M, or metal, layer is silver (Ag), the D, or dielectric, layer is titanium oxide (TiO_2), and the layer thicknesses are 33 nm, 28 nm, 30 nm, 28 nm, and 33 nm, respectively, as designed by Xu *et al.* [3]. The resulting EFC of the MDMDM unit cell at a free-space wavelength of 363.8 nm is roughly spherical with a radius approximately equal to the free-space wave number and a frequency gradient pointing toward the origin indicative of negative group velocity.[1] These features are consistent with the EFC of a left-handed Veselago medium with three-dimensionally isotropic refractive index $n = -1$. Effective constitutive parameters extracted from reflection and transmission data and Snell's law descriptions of simulated and measured refraction angles have also been shown to be consistent with this negative-refractive-index model [3]. This has led to the proposal that this metamaterial be characterized as a homogeneous medium with an isotropic left-handed response, a claim that has yet to be fully validated and will be thoroughly investigated in this paper.

Homogenization models have been successful in describing the properties of bilayered media with local or nonlocal dielectric tensors [6,20–23]. In such cases, the fundamental harmonics of the Floquet-Bloch modes are the dominant components and the modes resemble propagation in a homogeneous anisotropic dielectric medium. Therefore, the first question that arises regarding the validity of modeling the MDMDM structure with a single isotropic effective refractive index $n = -1$ is whether or not the propagating Floquet-Bloch modes can be described by single left-handed plane waves. For example, Fig. 2 illustrates snapshots of the magnetic field in the MDMDM unit cell at different points in time for energy propagation both parallel and perpendicular to the layers. Although the EFC of the unit cell suggests that it behaves like an isotropic and left-handed Veselago medium, the actual field distributions reveal complex wave dynamics that undermine this approximation. For propagation along the layers, the wave is a laterally confined mode that exhibits phase advancement opposing the direction of power flow. However, for propagation perpendicular to the layers, the wave exhibits an intricate and seemingly random field pattern from which a natural phase progression cannot be visually extracted. Examination of the field patterns for these two propagation directions suggests that the metamaterial may possess a left-handed response, but this response is likely not isotropic.

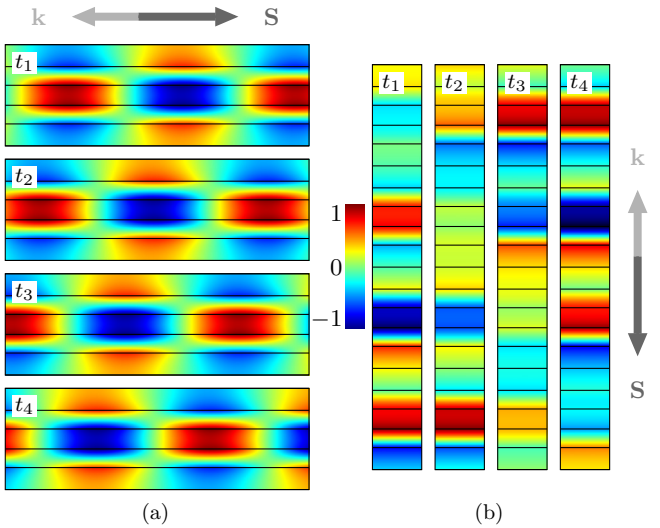

FIG. 2. Eigenmode magnetic field plots at quarter-period intervals over $t_1 < t_2 < t_3 < t_4$ for a wave propagating (a) parallel and (b) perpendicular to the planes. Wave attenuation has been removed for clarity. In (a), the net power flow is directed towards the right ($\hat{\mathbf{x}}$) while the mode phase propagates to the left ($-\hat{\mathbf{x}}$). In (b), the net power is directed downwards ($-\hat{\mathbf{z}}$) while the Floquet-Bloch phase propagates upwards ($\hat{\mathbf{z}}$). Note that although both configurations yield opposing Floquet-Bloch phase and power flow, the field distributions are strikingly different and a consistent phase progression across the mode can only be observed for the mode in (a).

III. MAPPING THE POWER FLOW OF FLOQUET-BLOCH HARMONICS

The limitation of effective medium theory and geometrical EFC analysis methods is that they assign the fundamental Floquet-Bloch wave vector as the wave vector of the global field and relate the total power flow to this harmonic without justification. In order to examine the validity of describing the MDMDM medium by a single isotropic refractive index $n = -1$, we propose instead a more complete description in which the internal electric and magnetic fields are decomposed into Floquet-Bloch harmonics [14,24,25] whose power flow is mapped in the spatial-frequency domain. For a periodic layered medium in which the layers are parallel to the xy plane, the periodic function $\mathbf{u}(z)$ can be expanded into a set of harmonic components distributed along a line parallel to the k_z axis with a spacing of $2\pi/a$. This enables both the magnetic field

[1] At this wavelength, the permittivities of the metamaterial layers were $\epsilon_{\mathrm{Ag}} = -2.522 + i0.251$ and $\epsilon_{\mathrm{TiO_2}} = 7.835 + i0.392$.

eigenmode from Eq. (1) and its corresponding electric field to be expressed in the spatial-frequency domain as the sum of Floquet-Bloch harmonics,

$$\mathbf{H}(\mathbf{r}) = \sum_m \mathbf{h}_m e^{i\frac{2\pi m}{a}z} e^{i\mathbf{k}_{\mathrm{FB}}\cdot\mathbf{r}}, \tag{3}$$

$$\mathbf{E}(\mathbf{r}) = \sum_m \mathbf{e}_m e^{i\frac{2\pi m}{a}z} e^{i\mathbf{k}_{\mathrm{FB}}\cdot\mathbf{r}}, \tag{4}$$

respectively, where a is the lattice constant of the layers along the z direction and m is an integer. In this formulation, $\mathbf{h}_m$ and $\mathbf{e}_m$ are the respective spatial Fourier transforms of the nonattenuating periodic components of the magnetic and electric field vectors. The harmonic components of the electric and magnetic fields each have a real wave vector given by $\mathbf{k}_m = \mathbf{k} + (2\pi m/a)\hat{\mathbf{z}}$ and an attenuation vector given by $\boldsymbol{\alpha} = \mathrm{Im}\{\mathbf{k}_{\mathrm{FB}}\}$, where $\mathbf{k} = \mathrm{Re}\{\mathbf{k}_{\mathrm{FB}}\}$ is the fundamental Floquet-Bloch wave vector. Pairing corresponding electric and magnetic field harmonics yields a spectrum of attenuating plane waves located at discrete real $\mathbf{k}_m$ points in the spatial-frequency domain (k space). We can find the bounded time-averaged Poynting vector of each individual Floquet-Bloch harmonic by considering only the nonattenuating components of the electromagnetic fields according to

$$\mathbf{S}_m = \tfrac{1}{2}\,\mathrm{Re}\{\mathbf{e}_m \times \mathbf{h}_m^*\}. \tag{5}$$

These vectors indicate the distribution of power flow across all harmonics, information which cannot be obtained from either graphical EFC analysis or effective medium theory.

Due to orthogonality of the harmonics $\frac{1}{a}\int_a \exp[i\mathbf{k}_m \cdot \mathbf{r}]\exp[-i\mathbf{k}_p \cdot \mathbf{r}]dz = \delta_{mp}$, the Poynting vectors of each harmonic are related to the Poynting vector of the nonattenuating component of the total fields by

$$\mathbf{S} = \frac{1}{v}\int_v \frac{1}{2}\,\mathrm{Re}\left\{\sum_m \mathbf{e}_m e^{i\mathbf{k}_m\cdot\mathbf{r}} \times \sum_p \mathbf{h}_p^* e^{-i\mathbf{k}_p\cdot\mathbf{r}}\right\} dv$$

$$= \sum_m \mathbf{S}_m, \tag{6}$$

where v is the volume of the unit cell. This confirms that the time-and-space-averaged power flow $\mathbf{S}$ of the global fields used in conventional modeling of the Floquet-Bloch mode with a single plane wave is the vector addition of the Poynting vectors of all the individual harmonics.

Mapping the harmonic Poynting vectors in k space provides an intuitive method to describe global field behavior without loss of information regarding the details of spatial field variations. Figure 3 illustrates the harmonic Poynting vectors in an infinitely periodic MDMDM medium for energy propagation parallel and perpendicular to the plane of the layers (corresponding to the cases considered in Fig. 2). In this analysis, the fields correspond to eigenmode solutions of Eq. (2), where the complex eigenvalue constraint $\mathbf{k}_{\mathrm{FB}} = \lambda\hat{\mathbf{k}}$ has been used to ensure a clearly defined direction of propagation $\hat{\mathbf{k}}$. For both the parallel and perpendicular cases, the three-dimensional distributions of the Poynting vectors are viewed from the top (projected onto the $k_x k_y$ plane) and from the side (projected onto the $k_x k_z$ plane). The black curve is the EFC of the layered metamaterial, the thick light-gray arrow is the fundamental Floquet-Bloch wave vector $\mathbf{k} = \mathrm{Re}\{\lambda\}\hat{\mathbf{k}}$,

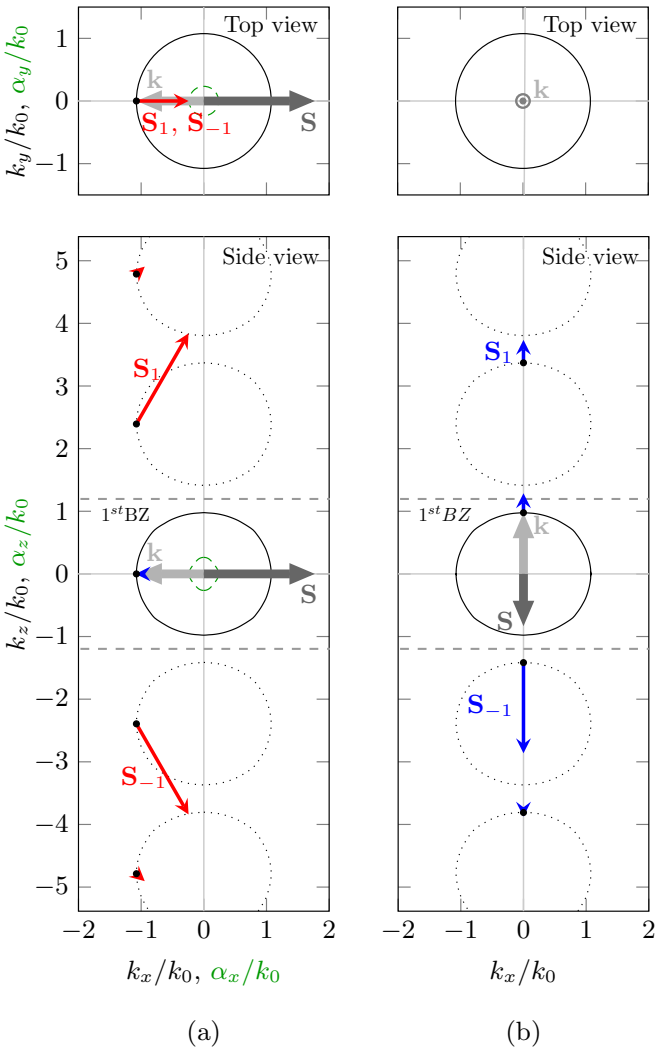

FIG. 3. The eigenmode fields are plotted in k space over the $k_x k_y$ plane (top panel) and over the $k_x k_z$ plane (bottom panel) for propagation parallel to the planes (a) and perpendicular to the planes (b). Left-handed plane-wave components in k space are plotted with red arrows, while right-handed components are plotted with blue arrows. The thick light-gray arrow is the Floquet-Bloch wave vector, and the thick dark-gray arrow is the Poynting vector of the total fields. The equifrequency contours corresponding to the real and imaginary parts of the calculated Floquet-Bloch wave vector are given by the black curve and the green dashed curve in (a), respectively. The first BZ is indicated by the light-gray dashed lines with the repeated EFCs arising from the periodicity of the structure plotted as dotted curves outside the first BZ. Note that the $\mathbf{S}_m$ vectors are not necessarily normal to their corresponding EFCs.

and the thick dark-gray arrow is the space- and time-averaged Poynting vector $\mathbf{S}$ of the global fields ($\mathbf{S}$ points in the direction of the frequency gradient of the EFC at point $\mathbf{k}$). The repeated EFCs arising from the periodicity of the structure are also plotted as dotted curves along the k_z axis at intervals of $2\pi/a$ outside the first BZ. The attenuation contours traced by the vector $\boldsymbol{\alpha} = \mathrm{Im}\{\lambda\}\hat{\mathbf{k}}$ are also plotted by the dashed green curves. These contours reveal an attenuation coefficient that is roughly isotropic, falling within the range of $0.22k_0$ to $0.26k_0$ as the direction of propagation changes. It can be observed

that the global fields generally consist of multiple plane-wave components whose Poynting vectors are not necessarily normal to their corresponding EFCs and that very little power lies within the first BZ. This confirms that no single plane-wave component (let alone the weak component lying in the first BZ) can be assigned to the global field. This demonstrates the importance of analyzing higher-order harmonics in the study of metamaterials and confirms that the MDMDM medium cannot be completely described by the repeated EFC diagrams [26] or effective constitutive parameters [27].

For in-plane propagation parallel to the layers, shown in Fig. 3(a), the fields decompose into a set of complementary plane-wave component pairs distributed symmetrically about the $k_x k_y$ plane. Each of these pairs can be interpreted as two plane waves bouncing back and forth within a waveguide formed by the unit cell. These "waveguide" modes form a standing wave in the transverse direction (perpendicular to the layers) and a propagating wave in the longitudinal direction (parallel to the layers). Because the longitudinal components of the Poynting vector and wave vector oppose each other, they form backward waves in that direction. This is consistent with the backward phase progression seen in Fig. 2(a). For out-of-plane propagation perpendicular to the layers, shown in Fig. 3(b), the fields decompose into a set of plane-wave components that have uneven Poynting vector magnitudes and are distributed at regular spatial-frequency intervals along the axis of propagation. Unlike the previous case of in-plane propagation, some plane-wave components propagate in the forward direction while others propagate in the backward direction. Interestingly, all components have power pointing in the same direction as phase. The most significant Floquet-Bloch harmonic is the higher-order $m = -1$ harmonic, which carries power and phase in the backward direction. The combination of all harmonics gives rise to the highly heterogeneous field pattern seen in Fig. 2(b), whose absence of discernible phase progression can now be explained by the multiple Floquet-Bloch wave components propagating in different directions.

As a single wave vector cannot generally be assigned to the global field, the handedness of the medium cannot be defined through the conventional practice of evaluating the sign of $\mathbf{k} \cdot \mathbf{S}$. On the other hand, each individual Floquet-Bloch harmonic has a well-defined wave vector and Poynting vector and can be classified as right or left-handed by first defining a reference axis in k space. This axis provides a consistent vector against which we can compare the directions of phase and power flow for each plane-wave component. The most meaningful way to establish this reference axis is to orient it to the fundamental Floquet-Bloch wave vector (whose direction is given by $\hat{\mathbf{k}}$), a vector which points from the origin to a spatial-frequency coordinate that is unique to the global fields. [This is also the direction in which Eq. (2) is initially solved.] The handedness of each plane-wave component can then be determined by the relative orientations of the Poynting vector and wave vector projected along this reference axis. When they oppose each other, the harmonic is classified as left-handed and indicated by a red arrow. When they are aligned with each other, the harmonic is classified as right-handed and indicated by a blue arrow. According to this scheme, the dominant plane-wave components for in-plane propagation are left-handed and the components for out-of-plane propagation perpendicular to the layers are right-handed, as shown in Fig. 3.

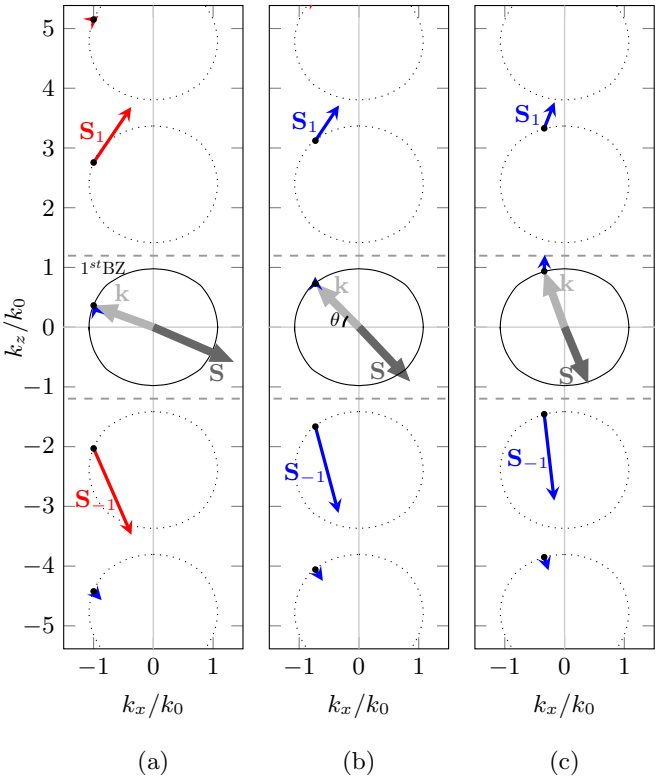

FIG. 4. The eigenmode fields are mapped to k space for modes propagating out of plane at an angle of (a) $\theta = 20°$, (b) $\theta = 45°$, and (c) $\theta = 70°$ with respect to the plane of the layers. Left-handed plane-wave components are plotted with red arrows, right-handed plane-wave components are plotted with blue arrows, the Floquet-Bloch wave vector is indicated by the thick light-gray arrow, and the total power flow is indicated by the thick dark-gray arrow. As θ increases, dominant contributors to power flow shift from left-handed to right-handed plane-wave components.

Figure 4 illustrates how wave propagation in the metamaterial smoothly evolves from resembling a backward waveguide mode for in-plane propagation to scattering with a dominant right-handed higher-order harmonic for out-of-plane propagation perpendicular to the layers. Power maps and dispersion diagrams are depicted for propagation angles of $\theta = 20°$, $45°$, and $70°$, where θ is defined as the angle between the reference axis ($\hat{\mathbf{k}}$) and the plane of the layers. Again, we observe that there is no significant power residing in the first BZ for all angles. The evolution of the harmonic Poynting vectors as a function of propagation angle is complicated. Whereas the Poynting vector $\mathbf{S}$ rotates with the propagation angle about the origin, the harmonic Poynting vectors rotate by smaller amounts, each in differing directions. The locations of the harmonic Poynting vectors are roughly anchored in k space, shifting by only small amounts versus propagation angle. Due to this property and the rotation of the reference axis, the plane-wave components change from being left-handed to right-handed as the direction of propagation goes from in plane to perpendicular out of plane. The changes in magnitude and direction of the harmonic Poynting vectors are consistent

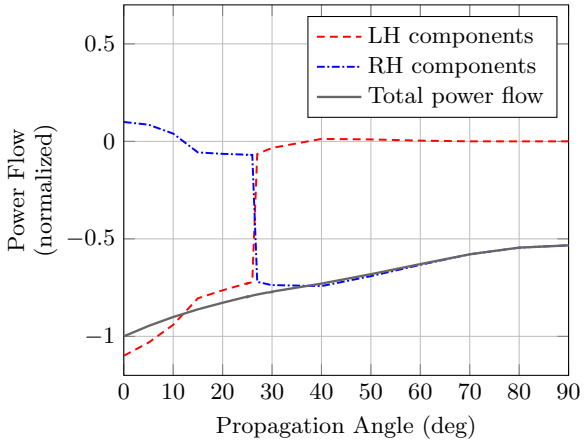

FIG. 5. Decomposition of total power flow along the reference direction into left-handed and right-handed contributions versus propagation angle θ. The dark gray trace plots the total power and is directly proportional to the group velocity, the red trace plots the power in the left-handed plane-wave components, and the blue trace plots the power in the right-handed plane-wave components. Propagation along the in-plane orientation ($\theta = 0^\circ$) is primarily left-handed and propagation along the out-of-plane perpendicular orientation ($\theta = 90^\circ$) is primarily right-handed.

with the evolution from waveguide modes with symmetric power maps (arising from transverse standing waves) for in-plane propagation, to asymmetric right-handed scattering for out-of-plane propagation in which power flows in the negative z direction.

Figure 5 compares the power-flow contributions along the reference axis from all left-handed components S_{LH} and all right-handed components S_{RH} as the propagation axis is tilted from in plane ($\theta = 0^\circ$) to perpendicular out of plane ($\theta = 90^\circ$). The field amplitudes have been normalized to achieve a constant energy density in the unit cell with respect to propagation direction. The summation of S_{RH} and S_{LH} yields the total power flow along the reference axis, which, due to the normalization process, is also proportional to the group velocity along the reference axis [28]. The negative value of the total power flow for all angles indicates all-angle negative group velocity, but here we see that it can arise from right-handed or left-handed plane-wave components. It can also be seen that the group velocity magnitude decreases for larger angles, which is consistent with the increasing presence of standing waves made of counterpropagating plane-wave components. This provides further evidence of the general electromagnetic anisotropy of this structure. For a given propagation direction, the relative contributions of S_{LH} and S_{RH} can be used to determine the origin of backward power (with respect to $\mathbf{k}_{\mathrm{FB}}$) and consequently distinguish between backward power flow and left-handedness. The origin of backward power and negative refraction of power is predominantly left-handed for small angles and right-handed for large angles. The sharp threshold between the left-handed and right-handed regimes arises because the dominant plane-wave components switch between left-handed and right-handed classifications at similar angles.

IV. ANALYSIS OF REFRACTION ACROSS AIR-METAMATERIAL INTERFACES

As previously discussed, the EFC of the layered plasmonic metamaterial is roughly spherical with a radius equal to the wave number in free space in which power flow opposes the fundamental Floquet-Bloch wave vector for all angles of propagation. The conventional conclusion would therefore be that this metamaterial can be modeled as an effective homogeneous left-handed medium with a three-dimensionally isotropic effective refractive index $n = -1$. Based on conventional EFC analysis, refraction into that medium from a homogeneous medium would be graphically described by drawing the EFCs at the working frequency and invoking continuity of the tangential wave-vector components across the interface [26]. Using this graphical procedure, or using Snell's law with the effective index $n = -1$, we would predict that waves incident from air onto a metamaterial facet of any orientation would undergo negative refraction of both power and phase for all angles of incidence. In other words, the Poynting and wave vectors would refract to the same side of the interface normal with an angle roughly equal to the angle of the incident wave. This refraction analysis, however, is valid only if the Floquet-Bloch mode propagating in the MDMDM can be described by a single plane wave located at the first BZ.

In order to achieve insight into the refractive behavior at the interface of the MDMDM medium, we expand the conventional analysis method by considering the power flow of all harmonic components of the Floquet-Bloch mode excited by the incident wave. The mode excited in the MDMDM structure is found by solving Eq. (2) while enforcing the continuity of the tangential wave vector at the interface. The Floquet-Bloch wave vector is written in terms of the eigenvalue λ as $\mathbf{k}_{\mathrm{FB}} = \mathbf{k}_{\mathrm{t}} + \lambda\hat{\mathbf{k}}_{\mathrm{n}}$, where $\mathbf{k}_{\mathrm{t}}$ is the tangential component of the incident wave vector and $\hat{\mathbf{k}}_{\mathrm{n}}$ is the unit normal. Figure 6 illustrates examples of refraction in three unique configurations: in-plane refraction at end-fire [across a planar interface perpendicular to the layers, as shown in Fig. 1(a)] with $\mathbf{k}_{\mathrm{t}} = k_{\mathrm{y}}\hat{\mathbf{y}}$ and $\hat{\mathbf{k}}_{\mathrm{n}} = \hat{\mathbf{x}}$, out-of-plane refraction at end-fire [Fig. 1(b)] with $\mathbf{k}_{\mathrm{t}} = k_z\hat{\mathbf{z}}$ and $\hat{\mathbf{k}}_{\mathrm{n}} = \hat{\mathbf{x}}$, and out-of-plane refraction at broadside [across a planar interface parallel to the layers, as shown in Fig. 1(c)] with $\mathbf{k}_{\mathrm{t}} = k_{\mathrm{x}}\hat{\mathbf{x}}$ and $\hat{\mathbf{k}}_{\mathrm{n}} = \hat{\mathbf{z}}$. The real and imaginary parts of the eigenvalue correspond to the normal component of the wave vector $k_{\mathrm{n}} = \mathrm{Re}\{\lambda\}$ and the attenuation coefficient $\alpha = \mathrm{Im}\{\lambda\}$, respectively. The direction of phase propagation is determined by the wave-vector components k_{t} and k_{n}, and the direction of attenuation is normal to the interface. The real and imaginary parts of the fundamental wave vector $\mathbf{k}_{\mathrm{FB}}$ are plotted in Fig. 6 for various interfaces as a function of k_{t} using black and green contours, respectively. Note that for incidence angles close to normal, there is very good agreement between these contours and the quasispherical EFCs from the infinite medium plotted in Fig. 3.

For each interface depicted in Fig. 6, the spatial-frequency maps of power flow are displayed for the mode corresponding to a plane wave incident from air at an angle of 20° with respect to the interface normal (i.e., the mode with $k_{\mathrm{t}} = k_0 \sin 20^\circ$). The real part of the fundamental Floquet-Bloch wave vector $\mathbf{k} = \mathbf{k}_{\mathrm{t}} + \mathbf{k}_{\mathrm{n}}$ is refracted at an angle of approximately 20° to the same side of normal as the incident wave vector.

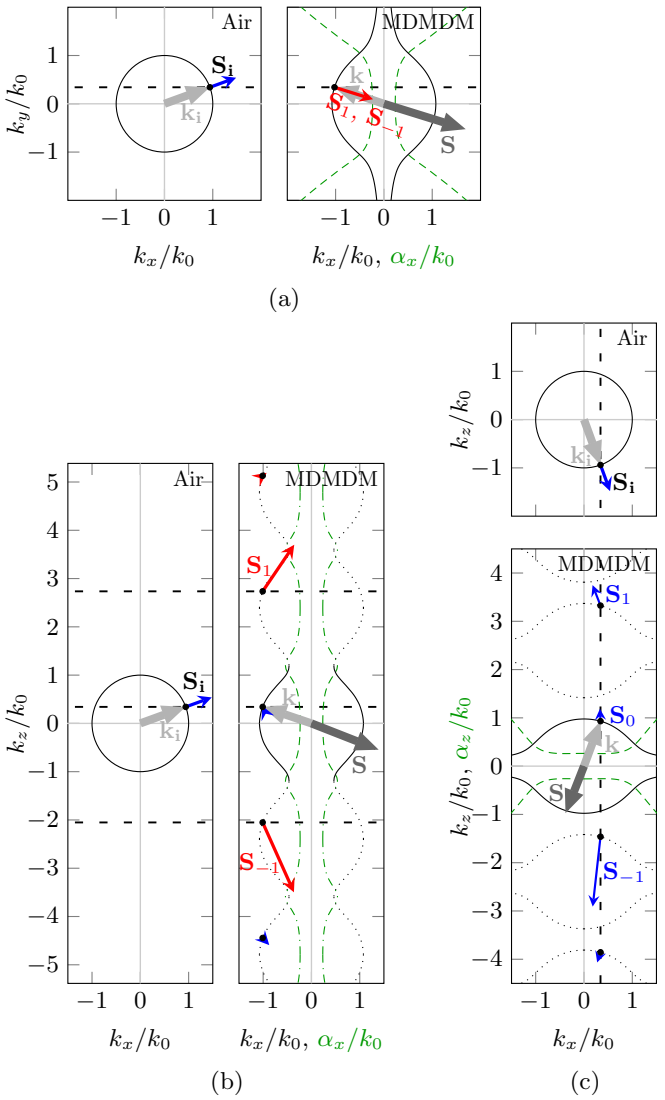

FIG. 6. Description of wave refraction from free space into the layered MDMDM structure based on the k-space components of the eigenmodes in the metamaterial and conservation of tangential wave vectors along the interface for (a) end-fire in-plane refraction, (b) end-fire out-of-plane refraction, and (c) broadside (out-of-plane) refraction. The wave number k_n and attenuation coefficient α of the fundamental wave vector $\mathbf{k}_{FB}$ in the direction normal to the interface are plotted with respect to the tangential wave number k_t using black and green (dashed) contours, respectively. Continuity of the tangential wave-vector components can be visualized through the black dashed lines. In the case of out-of-plane refraction at end-fire, the tangential wave-vector components of the higher-order harmonics appear outside the first BZ and only the fundamental component of the MDMDM wave is phase matched to the incident wave.

The average power flows away from the interface into the metamaterial with the averaged Poynting vector $\mathbf{S}$ pointing directly opposite to $\mathbf{k}$. Since conventional EFC analysis uses only $\mathbf{k}$ and $\mathbf{S}$ to model the power and phase behavior of the eigenmodes, it would predict negative refraction of both power and phase at the interfaces. Including the Poynting vector of each individual Floquet-Bloch harmonic projected onto the plane of incidence, however, indicates that the nature of refraction at an air-metamaterial interface is highly dependent on the orientations of the facet and plane of incidence. Negative phase and power refraction is unambiguously achieved only under in-plane end-fire illumination [Fig. 6(a)]. For out-of-plane refraction either by end-fire [Fig. 6(b)] or broadside [Fig. 6(c)] illumination, the refracted wave consists of multiple plane-wave components in which the dominant components are outside the first BZ. Vector summation of the harmonic Poynting vectors for both out-of-plane cases is consistent with negative power refraction, but phase refraction is ambiguous due to the presence of multiple plane-wave components. Figure 6(c) demonstrates that both the negative refraction of power observed experimentally and the double-negative parameters extracted from reflection and transmission data at the broadside interface of an MDMDM metamaterial slab [3] originates from refraction of higher-order right-handed $m = -1$ components, not from left-handedness.

V. MODE EXCITATION EFFICIENCY FOR OUT-OF-PLANE END-FIRE INCIDENCE

Our spatial-frequency maps suggest that it is possible to significantly enhance coupling into the metamaterial by wave-vector matching to the high-order harmonics. For end-fire illumination, the Floquet-Bloch harmonics of the eigenmode in the metamaterial have tangential wave-vector components given by

$$k_{m,z} = \mathbf{k}_m \cdot \hat{\mathbf{z}} = \mathbf{k} \cdot \hat{\mathbf{z}} + \frac{2\pi m}{a}. \tag{7}$$

These components are harmonics with a fundamental spacing given by the periodicity of the medium. Conservation of the tangential wave vector would imply that the metamaterial could be excited by an incident plane wave through any combination of these harmonics. It must also be noticed that the existence of such higher-order excitation channels is related to the periodicity of the MDMDM structure, and so they can also be predicted by conventional methods through the geometrical repetition of EFCs outside the first BZ [dotted EFCs at Fig. 6(b)]. However, the spatial-frequency power-flow maps further demonstrate that each channel corresponds to a particular harmonic with a specific contribution to the total power flow of the excited mode. Channels can therefore have different coupling efficiencies which cannot be determined by the simple geometrical repetition of EFCs in conventional methods [26]. Take, for example, the k-space map in Fig. 3(a) for an in-plane MDMDM mode (corresponding to $\theta = 0°$, or equivalently, $k_t = 0$), which shows that the two first-order harmonics ($m = \pm 1$) carry 78% of the total mapped x-directed power, whereas the fundamental harmonic ($m = 0$) carries less than 1%. A normally incident plane wave phase matched to the fundamental generally should yield low coupling efficiency into the structure, an observation that has been noted by others and has been attributed to impedance mismatch at the interface [2]. On the other hand, an incident plane wave matched to the $m = \pm 1$ components should yield significantly greater coupling efficiency. Note that power is conserved through the total power flow, regardless of the direction of the individual harmonic Poynting vector associated with a given excitation channel.

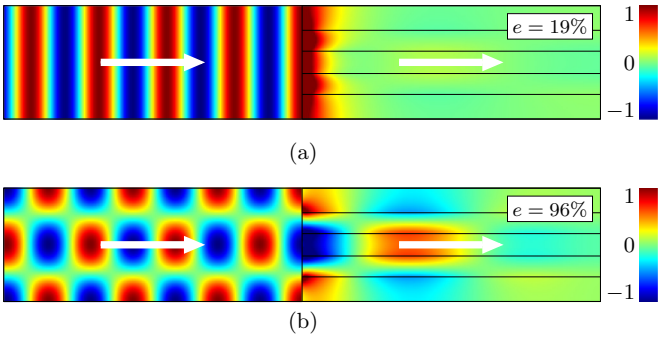

FIG. 7. The incident and transmitted magnetic field is plotted to show the coupling efficiency e for two different end-fire wave excitations of the normal in-plane MDMDM mode ($k_t = 0$). In (a), a normally incident plane-wave targets the $m = 0$ component of the MDMDM mode, while in (b), two oblique plane waves with incidence angles of $\pm 53.2^\circ$ are superposed in order to simultaneously target the $m = \pm 1$ components of the MDMDM mode. The white arrows show the direction of the time-and-space-averaged power flow in both the incidence dielectric medium ($n = 4$) and the layered medium. It is shown that coupling to the higher-order harmonics (the dominant k-space components) has increased the coupling efficiency by 505%.

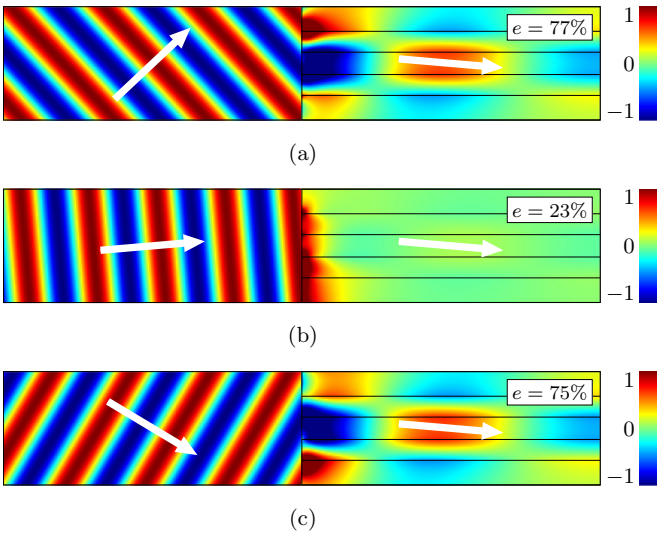

FIG. 8. The incident and transmitted magnetic field is plotted to show the coupling efficiency e for three different end-fire wave excitations of the out-of-plane MDMDM mode with $k_t = k_0 \sin 20^\circ$. In each plot, a plane wave is incident from a dielectric medium of index $n = 4$ with an angle (a) -43.1°, (b) -4.9°, and (c) 30.9° in order to target the $m = +1$, $m = 0$, and $m = -1$ component of the MDMDM mode, respectively. The coupling efficiency is shown to have increased by 326%–335% by coupling to the higher-order harmonics. The direction of power flow indicated by the white arrows demonstrates negative refraction of power at the interface for (a) and (b), and positive refraction of power for (c).

Our analysis suggests that the low coupling efficiency is related to field pattern mismatch at the interface, rather than impedance mismatch. To test this hypothesis, we consider the case of a dielectric-metamaterial interface under end-fire illumination in which the refractive index of the dielectric medium is sufficiently high ($n = 4$) to enable an incident plane wave to phase match to the first-order harmonics of the eigenmode. Changing the angle of incidence enables an incident plane wave to phase match to either the fundamental ($m = 0$) harmonic or one (or both) of the first-order ($m = \pm 1$) harmonics of the eigenmode. Using a combination of multiple incident plane waves, multiple harmonics can be phase matched simultaneously. To quantify the coupling efficiency of different excitation channels, we carry out full-wave simulations of wave incidence from a dielectric half space onto an MDMDM half space using COMSOL MULTIPHYSICS. The coupling efficiency is determined by the ratio of the transmitted power to the incident power in the direction normal to the interface.

Figure 7 plots the magnetic field distributions for end-fire normal illumination of the in-plane MDMDM mode (corresponding to $k_t = 0$) using two different excitation channels: one using a normally incident plane wave phase matched to the $m = 0$ component and another using two oblique plane waves phase matched to the $m = \pm 1$ components. The left half of each panel plots the incident fields, and the right half of each panel plots the transmitted fields. The direction of the time-and-space-averaged power flow is shown by the white arrows and the reflected fields have been omitted for clarity. Both excitation methods couple to the same eigenmode, which carries power and phase in opposing directions. The spatial field distribution of the transmitted mode for both cases is consistent with that of the in-plane eigenmode plotted in Fig. 2(a), except that the mode is now launched from an interface and attenuates heavily into the lossy MDMDM medium. The coupling efficiency for normal incidence excitation is 19%, whereas the coupling efficiency for oblique excitation is 96%. This corresponds to a transmittance increase of 505% and a reflectance reduction of more than 95%. The dramatic improvement in coupling efficiency confirms that the relative power maps are visceral and, in addition to clarifying the spatial-frequency distribution of power, can be used as means to obtain highly efficient excitation channels across interfaces.

The presence of multiple excitation channels means that it is possible for different plane waves to excite the same eigenmode. Figure 8 illustrates three different incident plane waves that excite the same $k_t = k_0 \sin 20^\circ$ mode within the MDMDM, albeit with different efficiencies. The angles of incidence are selected to be -43.1°, -4.9°, and 30.9° to achieve phase matching to the $m = +1$, $m = 0$, and $m = -1$ components, respectively, where a positive angle of incidence is measured in the clockwise direction from the interface normal ($-x$ axis). Illumination tailored to the $m = 0$ harmonic yields only 23% coupling efficiency into the medium. Illumination tailored to the $m = +1$ and $m = -1$ harmonics, on the other hand, yields coupling efficiencies of 77% and 75%, respectively. This corresponds to a transmittance increase of 326%–335% and a reflectance decrease of 68%–70%. Again, this result is consistent with the dominant power flow of the two first higher-order harmonics in the $k_t = k_0 \sin 20^\circ$ eigenmode given in Fig. 6(b).

Interestingly, the possibility of multiple excitation channels challenges the notion that refraction angles across a metamaterial interface can be uniquely defined. As shown by the white refracted arrows in Fig. 8, an incident wave that is

inclined at either positive or negative angles can excite the same eigenmode. Illumination phase matched to the $m = 0$ and $m = +1$ harmonics results in negative refraction of power, but with different angles of incidence. On the other hand, illumination phase matched to the $m = -1$ harmonic results in positive refraction of power. Clearly, such refractive behavior cannot be accurately described by assigning a single refractive index value to the metamaterial and invoking Snell's law.

VI. CONCLUSION

We have shown the importance of analyzing higher-order Floquet-Bloch harmonics when studying metamaterials and the need for a method that goes beyond effective medium theory or conventional geometrical EFC analysis.

Based on power-flow maps of Floquet-Bloch harmonics in k space, we have observed that a coupled plasmonic waveguide metamaterial with a spherical EFC that resembles the Veselago medium and can achieve quasi-isotropic negative refraction of power does not have a three-dimensionally isotropic left-handed response. The material achieves backward power flow for all angles, but the origin of this power flow depends on the propagation direction, evolving from left-handed for in-plane propagation to right-handed for out-of-plane propagation perpendicular to the layers. Negative refraction of both power and phase occurs only for in-plane propagation. Negative refraction of power occurs for out-of-plane propagation, but the absence of consistent phase progression implies that phase refraction cannot be defined in this configuration. Furthermore, both the negative refraction of power (and flat lensing) observed experimentally and the double-negative extracted parameters at broadside incidence were shown to originate from right-handed higher-order components. We can conclude from this that despite the existence of backward plasmonic modes along the layers, spherical EFCs, double-negative extracted effective parameters, and experimentally observed all-angle negative refraction of light beams, a sufficient condition for considering the layered structure as the realization of the homogeneous and isotropic left-handed Veselago medium has still not been met.

Due to existence of higher-order harmonics in the direction perpendicular to the layers, several excitation channels exist for end-fire illumination of the layered metamaterial. The efficiency of an excitation channel can be roughly predicted by the relative power residing in the corresponding harmonic. For example, we have shown that plane-wave coupling to the dominant first-order harmonics as opposed to the weak fundamental harmonic yields excitation efficiency enhancements of up to 505% for the in-plane MDMDM eigenmode. The presence of different excitation channels also means that it is possible for multiple incident waves to excite the same eigenmode, casting doubt on the practice of uniquely characterizing refraction angles across a metamaterial interface and then invoking Snell's law approximations.

In summary, mapping the power flow of Floquet-Bloch harmonics in k space provides a powerful tool to study the electromagnetic behavior of propagating modes within metamaterials. We have also shown that by quantifying the distribution of power across all harmonics, these power maps can provide a platform to engineer new ways to couple electromagnetic power into and out of metamaterial structures with high efficiency. These techniques have the potential to be applied to a range of electromagnetic problems, from the optimization of nanolenses for imaging and lithography to the design of novel structures for asymmetric power transmission.

ACKNOWLEDGMENTS

The authors acknowledge CMC Microsystems for the provision of CAD tools that facilitated this research. This work was supported by the Natural Sciences and Engineering Research Council of Canada (NSERC) through the Discovery Grants program.

[1] V. G. Veselago, Sov. Phys. Usp. **10**, 509 (1968).
[2] E. Verhagen, R. de Waele, L. Kuipers, and A. Polman, Phys. Rev. Lett. **105**, 223901 (2010).
[3] T. Xu, A. Agrawal, M. Abashin, K. J. Chau, and H. J. Lezec, Nature (London) **497**, 470 (2013).
[4] M. Notomi, Phys. Rev. B **62**, 10696 (2000).
[5] P. V. Parimi, W. T. Lu, P. Vodo, J. Sokoloff, J. S. Derov, and S. Sridhar, Phys. Rev. Lett. **92**, 127401 (2004).
[6] J. Schilling, Phys. Rev. E **74**, 046618 (2006).
[7] B. Wood, J. B. Pendry, and D. P. Tsai, Phys. Rev. B **74**, 115116 (2006).
[8] A. Salandrino and N. Engheta, Phys. Rev. B **74**, 075103 (2006).
[9] Y. Xiong, Z. Liu, and X. Zhang, Appl. Phys. Lett. **93**, 111116 (2008).
[10] T. Xu, Y. Zhao, J. Ma, C. Wang, J. Cui, C. Du, and X. Luo, Opt. Express **16**, 13579 (2008).
[11] G. Zheng, S. Xiao, C. Zhang, W. Su, and Y. Liu, Optik (Munich, Ger.) **124**, 4780 (2013).
[12] F. Bilotti, S. Tricarico, and L. Vegni, IEEE Trans. Nanotechnol. **9**, 55 (2010).
[13] I. Aghanejad, K. Chau, and L. Markley, in *2015 IEEE International Symposium on Antennas and Propagation USNC/URSI National Radio Science Meeting, Vancouver, BC, Canada* (IEEE, New York, 2015), pp. 657–658.
[14] B. Lombardet, L. A. Dunbar, R. Ferrini, and R. Houdré, J. Opt. Soc. Am. B **22**, 1179 (2005).
[15] L. Markley, Phys. Rev. B **94**, 085108 (2016).
[16] K. Sakoda, *Optical Properties of Photonic Crystals*, 2nd ed. (Springer, New York, 2004).
[17] J. D. Joannopoulos, S. G. Johnson, J. N. Winn, and R. D. Meade, *Photonic Crystals: Molding the Flow of Light*, 2nd ed. (Princeton University Press, Princeton, NJ, 2008).
[18] C. Fietz, Y. Urzhumov, and G. Shvets, Opt. Express **19**, 19027 (2011).
[19] http://www.comsol.com.

[20] P. Shekhar, J. Atkinson, and Z. Jacob, Nano Convergence **1**, 1 (2014).
[21] A. V. Chebykin, A. A. Orlov, A. V. Vozianova, S. I. Maslovski, Y. S. Kivshar, and P. A. Belov, Phys. Rev. B **84**, 115438 (2011).
[22] A. V. Chebykin, A. A. Orlov, C. R. Simovski, Y. S. Kivshar, and P. A. Belov, Phys. Rev. B **86**, 115420 (2012).
[23] R.-L. Chern, Opt. Express **21**, 16514 (2013).
[24] R. Maas, E. Verhagen, J. Parsons, and A. Polman, ACS Photonics **1**, 670 (2014).
[25] K. J. Chau, M. H. Al Shakhs, and P. Ott, Prog. Electromagn. Res. Symp. **40**, 45 (2014).
[26] S. Foteinopoulou and C. M. Soukoulis, Phys. Rev. B **72**, 165112 (2005).
[27] C. Menzel, C. Rockstuhl, T. Paul, F. Lederer, and T. Pertsch, Phys. Rev. B **77**, 195328 (2008).
[28] L. D. Landau, E. M. Lifshitz, and L. P. Pitaevski, *Electrodynamics of Continuous Media*, 2nd ed. (Butterworth-Heinenan, Oxford, 1984).